Deep Learning for Spectrum Prediction From Spatial–Temporal–Spectral Data

Xi Li, *Member, IEEE*, Zhicheng Liu, *Graduate Student Member, IEEE*, Guojun Chen, *Graduate Student Member, IEEE*, Yinfei Xu, *Member, IEEE*, and Tiecheng Song, *Member, IEEE*

***Abstract*— Spectrum prediction is challenging owing to its complex inherent dependency and heterogeneity among the spectrum data. In this letter, we propose a novel end-to-end deep-learning-based model, entitled spatial-temporal-spectral prediction network (STS-PredNet), to collectively predict the states of various frequency bands in all locations of interest at the same time. More specifically, the predictive recurrent neural network (PredRNN) is trained to capture the spatial-temporal-spectral dependencies of spectrum data. Three components of PredRNN units are employed to model the three kinds of temporal properties in spectrum data, i.e. closeness, daily period, and weekly trend. The final prediction is then performed in a dynamically aggregated way. Extensive experiments are conducted based on a real-world spectrum measurement dataset, which illustrate the superiority of the proposed STS-PredNet over the state-of-the-art baselines.**

***Index Terms*— Cognitive radio, deep learning, dynamic spectrum access, spectrum prediction.**

I. Introduction

SPECTRUM prediction is a way of inferring relevant information about future spectrum usage from measured spectrum data. It can provide forecast views of the spectrum usage pattern of various wireless services and has a wide range of applications in wireless networks. For example, it has been well known that adopting spectrum prediction can enable dynamic spectrum access, enhance spectrum utilization efficiency, and finally alleviate the contradiction between spectrum shortage and spectrum under-utilization [1]. The research on spectrum prediction has received increasing attention during the past few years. A number of spectrum prediction techniques, such as models based on linear regression analysis, Bayesian inference and matrix/tensor completion [2], have been proposed.

Space, time, frequency dimensions of spectrum usage pattern are complex due to various factors such as radio propagating environment, user mobility and diverse user requirements. To capture the complex dependencies among the measured spectrum data, recent advances on deep learning models have established themselves as strong competitors to classical statistical models for spectrum prediction. Aiming at exploiting the spatial dependence, temporal dependence or spectral dependence of the spectrum data, long short-term memory (LSTM) model [3], convolutional neural network (CNN) [4], convolutional LSTM (ConvLSTM) model [5], deep transfer learning algorithm [6], and a hierarchical learning system of both a fine-tuned CNN and a gated recurrent unit network (GRU) [7], etc., have already been developed for spectrum prediction. However, even with such plenty of applications of deep learning approaches in spectrum prediction, the work on dealing with the joint spatial-temporal-spectral dependencies in spectrum data is limited. Besides, spectrum data show cyclical patterns due to the effect of human daily routine. We can easily observe temporal closeness, daily period and weekly trend from the real-world spectrum data [8]. The above works perform spectrum prediction without considering the temporal diversity of the spectrum data, resulting in inadequate modeling and unsatisfactory prediction performance.

Motivated by the aforementioned problems, this letter proposes a new deep-learning-based spatial-temporal-spectral prediction network, entitled by STS-PredNet, for signal-power-level spectrum prediction, i.e., prediction of the signal power level on a specific channel at a specific location to define the quality. More specifically, the predictive recurrent neural network (PredRNN) [9], which is the most advanced ConvLSTM architecture, is firstly introduced into the spectrum prediction domain. STS-PredNet adopts PredRNN to effectively model the spatial, temporal and spectral dependencies of the spectrum data. Three components based on the PredRNN are designed to model the temporal closeness, daily period and weekly trend, respectively. STS-PredNet dynamically aggregates the outputs of the three components, assigning different weights according to their contributions. Experimental results verify that STS-PredNet can significantly improve the predictive performance, and provide stable and accurate prediction results for different prediction ranges.

II. Problem Statement

In a typical centralized cognitive radio (CR) network, K sparsely distributed secondary users (SU) are continuously monitoring F frequency bands and sending their received signal strengths (RSS) to a fusion center (FC). At each time t,

Manuscript received November 21, 2020; accepted December 11, 2020. Date of publication December 16, 2020; date of current version April 9, 2021. The work was supported by the National Natural Science Foundation of China under Grant 61771126, Grant 61901105, and Grant 52078117, the Natural Science Foundation of Jiangsu Province under Grant BK20190343. The associate editor coordinating the review of this letter and approving it for publication was G. Brante. *(Corresponding author: Yinfei Xu.)*

Xi Li, Guojun Chen, and Tiecheng Song are with the National Mobile Communications Research Laboratory, Southeast University, Nanjing 210096, China (e-mail: lixixuzhou@seu.edu.cn; guojunchen@seu.edu.cn; songtc@seu.edu.cn).

Zhicheng Liu and Yinfei Xu are with the School of Information Science and Engineering, Southeast University, Nanjing 210096, China (e-mail: zhichengliu@seu.edu.cn; yinfeixu@seu.edu.cn).

Digital Object Identifier 10.1109/LCOMM.2020.3045205

a spectrum map $\mathbf{X}_t \in \mathbb{R}^{N\times F}$ can be constructed at the FC to be referred for the signal power strength of F frequency bands at N locations in the spatial region of interest. Each element of $\mathbf{X}_t$ is calculated by fusing the RSSs of the K SUs. In this letter, we have chosen to linearly combine the RSSs of the SUs using the well-known inverse distance weighting (IDW) method as [5]

$$\mathbf{X}_t\left(n,f\right)=\sum_{k=1}^{K}\omega_{n,k}\cdot r_{f,t}^{k}, \tag{1}$$

where $r_{f,t}^{k}$ denotes the RSS of the f^{th} frequency band sensed by the k^{th} SU at time t and $\omega_{n,k}$ is the corresponding weighting coefficient, which can be expressed as

$$\omega_{n,k}=\frac{\left(d_{n,k}\right)^{-\alpha}}{\sum_{j=1}^{K}\left(d_{n,j}\right)^{-\alpha}}, \tag{2}$$

where $d_{n,k}$ represents the Euclidean distance between the k^{th} SU and the n^{th} location of interest, $\alpha=2$ is a path-loss exponent.

The goal of spectrum prediction in this letter is to predict the most probable $\mathbf{X}_{T+\triangle t}$ in the future given the T-length historical spectrum map sequence $\{\mathbf{X}_t|t=1,\ldots,T\}$ as

$$\widehat{\mathbf{X}}_{T+\triangle t}=\arg\max_{\mathbf{X}_{T+\triangle t}} p\left(\mathbf{X}_{T+\triangle t}|\mathbf{X}_1,\ldots,\mathbf{X}_T\right), \tag{3}$$

where $\triangle t$ is the length of the time interval between the latest constructed spectrum map and the predicted one, which also represents the prediction range.

III. Deep Spatial-Temporal-Spectral Prediction Network

A. Preliminaries

Three kinds of temporal properties, i.e., closeness, daily period and weekly trend, can be easily observed from real-world spectrum data. These properties are the results of user demand regularity and user demand deviation [10], [11]. An illustrative example using the RSSs of a certain broadcasting TV channel sensed by an Electrosense sensor located in Madrid, Spain [8], is presented in Fig. 1.

- **Closeness**: Fig. 1(a) shows the ratio curve of the RSSs, where x-axis is the time interval between two spectrum sensing timeslots and y-axis is the average ratio value between arbitrary two RSSs that have the same time interval. Obviously, current RSS is more relevant to recent historical RSSs than the distant ones, which implies temporal closeness.
- **Daily period**: Fig. 1(b) depicts RSSs at all spectrum sensing timeslots of 7 days from May 11, 2020 to May 17, 2020, where daily periodicity in spectrum data can be easily noticed.
- **Weekly trend**: Fig. 1(c) describes RSSs at a certain spectrum sensing timeslot (14:00pm-14:10pm) of Thursday from April 2020 to June 2020. We can see the obvious weekly trend that the RSS progressively decreases as time goes by.

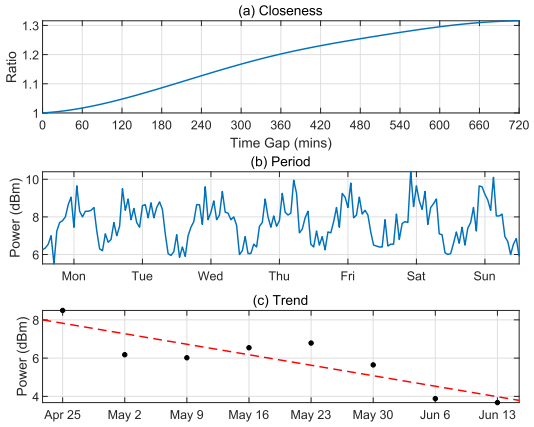

Fig. 1. Three kinds of temporal properties of spectrum data, i.e., closeness, daily period, and weekly trend.

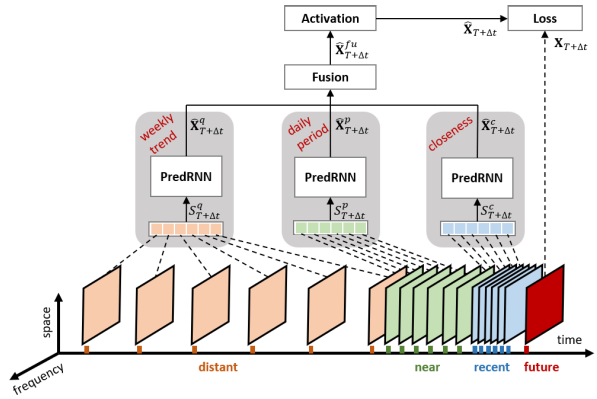

Fig. 2. Architecture of STS-PredNet.

B. Architecture of STS-PredNet

Inspired by the above observations on temporal properties, we propose a novel deep-learning-based model, entitled by STS-PredNet, to solve the spectrum prediction problem. Fig. 2 displays the overall architecture of STS-PredNet. Leveraging the end-to-end architecture [12], STS-PredNet is composed of three major components modeling temporal closeness, daily period and weekly trend, respectively. The three components share the same network structure with a PredRNN to capture the joint spatial-temporal-spectral dependencies based on recent/near/distant historical spectrum data. The outputs of the three components are then aggregated based on parameter matrices, which are learnable to reflect the difference of the contributions of the three temporal properties. Finally, the aggregation result is followed by an activation function.

C. Structure of the Three Components

The joint spatial-temporal-spectral dependencies observed in the spectrum data can be viewed as a complex higher-order learning problem for LSTM networks. ConvLSTM, which takes advantage of both CNN and LSTM, is able to model the multi-dimensional dependencies of the spectrum data [5]. In this letter, we introduce the most advanced ConvLSTM, entitled by PredRNN [9], in each component of our STS-PredNet to acquire the joint spatial-spectral features and effectively analyze temporal dependencies for spectrum prediction.

The PredRNN adopts the encoder-decoder RNN architecture that is proposed in [13]. As illustrated in Fig. 3, for a PredRNN composed of L-layer stacked spatial-temporal-spectral ConvLSTM (STS-ConvLSTM) units, highly abstract features are extracted layer-by-layer through convolution operations with hidden states $\mathbf{H}$ being delivered from bottom to top. Apart from the standard memory cells $\mathbf{C}$ which are constrained inside each STS-ConvLSTM unit and be updated merely in time domain (denoted by horizontally black arrows), a unified memory cell $\mathbf{M}$ is applied to be shared by all the STS-ConvLSTM units in PredRNN. The unified memory cell is updated along a zigzag direction (denoted by orange arrows) to convey the memory both vertically across layers and horizontally over time. With the aid of the unified memory cell, PredRNN enables efficient flow of spatial-temporal-spectral information, overcoming the drawbacks of the layer-independent memory mechanism of the conventional ConvLSTM architecture. PredRNN determines the future state of a certain STS-ConvLSTM unit by the inputs and past states. This can be easily achieved by exploiting convolutions in both input-to-state and state-to-state transitions. The key equations that define STS-ConvLSTM for a given input $\mathbf{X}_t$ are given as follows:

$$\mathbf{g}_t = \tanh\left(\mathbf{W}_{xg} * \mathbf{X}_t + \mathbf{W}_{hg} * \mathbf{H}_{t-1}^{l} + \mathbf{b}_g\right); \quad (4)$$

$$\mathbf{i}_t = \sigma\left(\mathbf{W}_{xi} * \mathbf{X}_t + \mathbf{W}_{hi} * \mathbf{H}_{t-1}^{l} + \mathbf{b}_i\right); \quad (5)$$

$$\mathbf{f}_t = \sigma\left(\mathbf{W}_{xf} * \mathbf{X}_t + \mathbf{W}_{hf} * \mathbf{H}_{t-1}^{l} + \mathbf{b}_f\right); \quad (6)$$

$$\mathbf{C}_t^l = \mathbf{f}_t \odot \mathbf{C}_{t-1}^l + \mathbf{i}_t \odot \mathbf{g}_t; \quad (7)$$

$$\mathbf{g}'_t = \tanh\left(\mathbf{W}'_{xg} * \mathbf{X}_t + \mathbf{W}_{mg} * \mathbf{M}_t^{l-1} + \mathbf{b}'_g\right); \quad (8)$$

$$\mathbf{i}'_t = \sigma\left(\mathbf{W}'_{xi} * \mathbf{X}_t + \mathbf{W}_{mi} * \mathbf{M}_t^{l-1} + \mathbf{b}'_i\right); \quad (9)$$

$$\mathbf{f}'_t = \sigma\left(\mathbf{W}'_{xf} * \mathbf{X}_t + \mathbf{W}_{mf} * \mathbf{M}_t^{l-1} + \mathbf{b}'_f\right); \quad (10)$$

$$\mathbf{M}_t^l = \mathbf{f}'_t \odot \mathbf{M}_t^{l-1} + \mathbf{i}'_t \odot \mathbf{g}'_t; \quad (11)$$

$$\mathbf{o}_t = \sigma\left(\mathbf{W}_{xo} * \mathbf{X}_t + \mathbf{W}_{ho} * \mathbf{H}_{t-1}^{l} + \mathbf{W}_{co} * \mathbf{C}_t^l \right. \quad (12)$$

$$\left. + \mathbf{W}_{mo} * \mathbf{M}_t^l + \mathbf{b}_o\right); \quad (13)$$

$$\mathbf{H}_t^l = \mathbf{o}_t \odot \tanh\left(\mathbf{W}_{1\times1} * \left[\mathbf{C}_t^l, \mathbf{M}_t^l\right]\right), \quad (14)$$

where σ is sigmoid activation function, $\tanh$ is hyperbolic tangent activation function, $*$ and $\odot$ denote the convolution operator and the Hadamard product respectively. The weights, $\mathbf{W}_g, \mathbf{W}_i, \mathbf{W}_f, \mathbf{W}_o$, corresponds to feature extracting convolutional filter matrices in $\mathbb{R}^{N\times F}$, used to transform in the state-to-state and input-to-state convolutional transitions. $\mathbf{C}_t^l \in \mathbb{R}^{N\times F}, (l \in \{1,\ldots,L\})$ is the standard cell state that is delivered horizontally from the previous time step to the current time step within each STS-ConvLSTM layer, while $\mathbf{M}_t^l \in \mathbb{R}^{N\times F}, (l \in \{1,\ldots,L\})$ is the unified memory that is conveyed vertically from the previous layer to the current layer at the same time step. For the bottom layer where $l = 1$, $\mathbf{M}_t^{l-1} = \mathbf{M}_{t-1}^L$. We construct another set of gate structure (i.e., $\mathbf{i}'_t$, $\mathbf{f}'_t$, and $\mathbf{g}'_t$) for $\mathbf{M}_t^l$, while maintaining the gates (i.e., $\mathbf{i}_t$, $\mathbf{f}_t$, and $\mathbf{g}_t$) for $\mathbf{C}_t^l$ as in standard ConvLSTM. At last, we concatenate the two kinds of memories together and then apply a 1×1 convolution layer for dimension reduction, which makes the hidden state $\mathbf{H}_t^l, (l \in \{1,\ldots,L\})$ of the same dimensions as the memory cells.

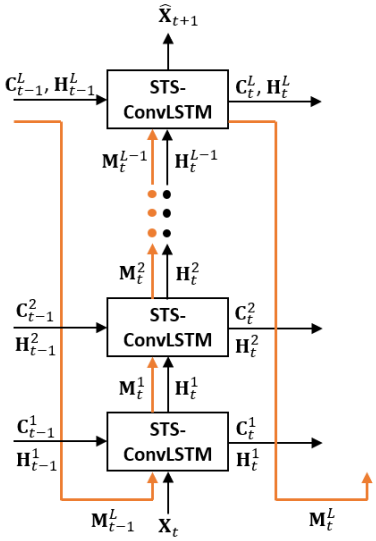

Fig. 3. PredRNN with L stacked STS-ConvLSTM units. The orange arrows in PredRNN denote the transition path of the unified memory $\mathbf{M}$.

The three components describing temporal closeness, daily period and weekly trend in Sec. III-B share the same PredRNN structure as discussed above. For the target $\mathbf{X}_{T+\triangle t}$ to be predicted, three kinds of subsequences are sampled from the T-length historical spectrum map sequence $\{\mathbf{X}_t | t = 1,\ldots,T\}$ to model the temporal closeness dependence, daily period dependence and weekly trend dependence respectively. Define l_c as the length of dependence of closeness, the spectrum maps of recent time segment modeling the temporal closeness dependence can be written as $\mathcal{S}_{T+\triangle t}^c = \left\{\mathbf{X}_{T-(l_c-1)}, \mathbf{X}_{T-(l_c-2)}, \ldots, \mathbf{X}_T\right\}$. Similarly, define l_p as the length of dependence of daily period, the spectrum maps of near history segment modeling the daily period dependence can be written as $\mathcal{S}_{T+\triangle t}^p = \left\{\mathbf{X}_{T+\triangle t-l_p\cdot p}, \mathbf{X}_{T+\triangle t-(l_p-1)\cdot p}, \ldots, \mathbf{X}_{T+\triangle t-p}\right\}$, where p is equal to one-day that describes daily periodicity. Likewise, define l_q as the length of dependence of weekly trend, the spectrum maps of distant history segment modeling the weekly trend dependence can be written as $\mathcal{S}_{T+\triangle t}^q = \left\{\mathbf{X}_{T+\triangle t-l_q\cdot q}, \mathbf{X}_{T+\triangle t-(l_q-1)\cdot q}, \ldots, \mathbf{X}_{T+\triangle t-q}\right\}$, where q is equal to one-week that reveals the weekly trend. With the inputs of $\mathcal{S}_{T+\triangle t}^c, \mathcal{S}_{T+\triangle t}^p, \mathcal{S}_{T+\triangle t}^q$, the outputs of the three components are respectively obtained as $\widehat{\mathbf{X}}_{T+\triangle t}^c, \widehat{\mathbf{X}}_{T+\triangle t}^p$, and $\widehat{\mathbf{X}}_{T+\triangle t}^q$.

D. Aggregation of the Three Components

Considering that the extent to the roles of temporal closeness, daily period and weekly trend is not globally the same for different locations and frequency bands, we employ a parametric-matrix-based fusion method [14] to aggregate the outputs of the three components (i.e., closeness, period, trend) as follows

$$\widehat{\mathbf{X}}_{T+\triangle t}^{fu} = \mathbf{W}_c \odot \widehat{\mathbf{X}}_{T+\triangle t}^c + \mathbf{W}_p \odot \widehat{\mathbf{X}}_{T+\triangle t}^p + \mathbf{W}_q \odot \widehat{\mathbf{X}}_{T+\triangle t}^q, \quad (15)$$

where $\mathbf{W}_c$, $\mathbf{W}_p$ and $\mathbf{W}_q$ are learnable parameters that reflect the degrees of temporal closeness influence, daily period influence and weekly period influence on the predicted target.

After aggregating the three components, we adopt an activation layer at the end of our model. Finally, the predicted value, denoted by $\widehat{\mathbf{X}}_{T+\triangle t}$, is defined as

$$\widehat{\mathbf{X}}_{T+\triangle t} = h\left(\widehat{\mathbf{X}}^{fu}_{T+\triangle t}\right), \tag{16}$$

where h is an activation function, e.g., the hyperbolic tangent function.

E. Training Algorithm

The STS-PredNet is trained by minimizing the mean squared error (MSE) between the true value and the predicted value as

$$\mathcal{L}(\theta) = \left\| \mathbf{X}_{T+\triangle t} - \widehat{\mathbf{X}}_{T+\triangle t} \right\|_2^2, \tag{17}$$

where θ are all learnable parameters in the STS-PredNet.

Algorithm 1 outlines the STS-PredNet training process. Firstly, training instances are constructed from the original spectrum map sequence using a sliding window scheme (lines 1-10). Then, forward propagation and back propagation are repeatedly applied to train the model (lines 11-16).

Algorithm 1 STS-PredNet Training Algorithm

Input: Historical spectrum data sequence $\{\mathbf{X}_t | t = 1, \ldots, T\}$; Lengths of closeness, period, trend subsequences: l_c, l_p, l_q; Prediction range: $\triangle t$.

Output: Learned STS-PredNet model.

1 $\Gamma \leftarrow \emptyset$;
2 // construct training instances;
3 $t_0 = \max\{l_c, (l_p+1)\cdot p - \triangle t, (l_q+1)\cdot q - \triangle t\}$;
4 **for** $t_0 \le t \le T - \triangle t$ **do**
5 $\quad \mathcal{S}^c_{t+\triangle t} = \{\mathbf{X}_{t-(l_c-1)}, \ldots, \mathbf{X}_t\}$;
6 $\quad \mathcal{S}^p_{t+\triangle t} = \{\mathbf{X}_{t+\triangle t-l_p\cdot p}, \ldots, \mathbf{X}_{t+\triangle t-p}\}$;
7 $\quad \mathcal{S}^q_{t+\triangle t} = \{\mathbf{X}_{t+\triangle t-l_q\cdot q}, \ldots, \mathbf{X}_{t+\triangle t-q}\}$;
8 $\quad$ // $\mathbf{X}_{t+\triangle t}$ is the target;
9 $\quad$ put a training instance $\left(\left\{\mathcal{S}^c_{t+\triangle t}, \mathcal{S}^p_{t+\triangle t}, \mathcal{S}^q_{t+\triangle t}\right\}, \mathbf{X}_{t+\triangle t}\right)$ into Γ;
10 **end**
11 // train the model;
12 initialize all learnable parameters θ in STS-PredNet;
13 **repeat**
14 $\quad$ randomly select a batch of instances Γ_b from Γ;
15 $\quad$ obtain the optimized θ by minimizing the objective (17) with Γ_b;
16 **until** *stopping criteria is met*;

IV. EXPERIMENTS

A. Settings

1) Dataset: In this section, numerical experiments are provided to evaluate the performance of the proposed method. An aggregated spectrum measurement dataset of 790 - 850 MHz frequency bands sensed by 4 Electrosense[1] sensors located in Madrid, Spain is used for the evaluations. The statistics of the dataset is described in Table I. We randomly select 100 locations in a 4 km^2 space area of interest,[2] and construct a spectrum map based on the measurement data as described in Sec. II. The size of the spectrum map can be easily obtained as $(100, 60)$. The spectrum map is updated every 10 minutes from 4th April, 2020 to 20th June, 2020. We split the spectrum map sequence in 10/2 ratio for network training and testing, respectively. For the sake of model training, we use the min-max normalization method to scale the data value into the range $[-1, 1]$. In the evaluation, we re-scale the predicted value back to the normal value, compared with the ground truth.

TABLE I
STATISTICS OF THE SPECTRUM MEASUREMENT DATASET

Dataset	Electrosense spectrum measurement data
Data type	Received signal power in dBm
Location	Madrid, Spain
Number of sensors	4 (test_yago, imdea_6ghz, imdea_adsb, Noelia)
Time span	4th Apr. 2020 - 20th Jun. 2020
Resolution time interval	10 mins
Frequency span	790 - 850 MHz
Resolution bandwidth	1 MHz

2) Hyperparameters: The PredRNN in the three components of our STS-PredNet consists of four STS-ConvLSTM layers with 128 hidden states each. The convolution filters inside the STS-ConvLSTM units are set to 3×3. Adam is used as the optimizer. The number of epochs and learning rate are set as 500 and 0.0002, respectively. The batch size is 32. In order to prevent overfitting in our STS-PredNet, we select 90% of the training data for training the model, and treat the remaining 10% as the validation set, which is used to early-stop our training algorithm based on the best validation score. For lengths of the three dependent sequences, we set them as $l_c = 36$, $l_p = 7$, $l_q = 4$.

3) Baselines and Evaluation Metrics: For comparison, 5 predictors are considered as baselines, which are (1) traditional prediction algorithms: historical average (HA) and Auto-regressive Integrated Moving Average (ARIMA) [12], and (2) deep-learning-based algorithms: LSTM [3], ConvLSTM [5], and STDenseNet [15]. Moreover, 4 valuation metrics, i.e., mean absolute percentage error (MAPE), mean absolute error (MAE), root mean square error (RMSE) [12], and R-squared (R^2) [16] are used to evaluate the performance.

B. Experimental Results and Discussions

We first give the comparison with baselines on short-term spectrum prediction. The prediction range is set as $\triangle t =$ 10 mins. We perform two versions of STS-PredNet, i.e., the original STS-PredNet that takes consideration of temporal closeness, daily period and weekly trend at the same time and a variant termed STS-PredNet-C that contains the closeness component only. Table II presents the prediction error (MAPE, MAE, RMSE), goodness-of-fit performance (R^2), time consumption required to complete a spectrum map prediction and

[1] https://electrosense.org/

[2] (2 km $\times$ 2 km) square area centering at [-3.76897, 40.33633].

TABLE II
VALUATION PERFORMANCE ON TEST SET

Model	MAPE	MAE	RMSE	R^2	Memory	Time
HA	13.11%	1.99	2.42	0.192	0B	10^{-4}s
ARIMA	6.04%	0.93	1.20	0.613	272B	10^{-4}s
LSTM	4.58%	0.81	1.02	0.937	156.2MB	0.077s
ConvLSTM	3.99%	0.75	1.14	0.990	284.1MB	0.176s
STDenseNet	4.00%	0.74	1.01	0.993	267.3MB	0.662s
STS-PredNet-C	**3.84%**	**0.72**	**0.98**	**0.994**	**319.7MB**	**0.178s**
STS-PredNet	**3.54%**	**0.63**	**0.87**	**0.995**	**412.0MB**	**0.863s**

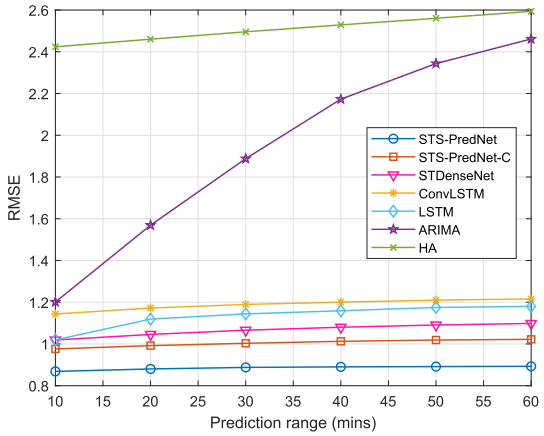

Fig. 4. Comparison of STS-PredNets with other baselines verses prediction range.

memory usage of the seven models. It can be observed that all the models have small prediction errors. However, due to the limited ability to deal with the complex dependencies among the spectrum data, the traditional prediction algorithms (HA and ARIMA) have larger MAPE/MAE/RMSE and worse R^2 than that of the deep-learning-based algorithms (LSTM, ConvLSTM, STDenseNet and the STS-PredNets). Among all the models, our STS-PredNets show the best performance in terms of all evaluation metrics at the expense of relatively higher time and space complexity. Moreover, our STS-PredNet has relatively 7.79% lower MAPE, 11.45% lower MAE and 11.02% lower RMSE than that of STS-PredNet-C, which verifies the effectiveness of considering temporal diversity for spectrum prediction.

Fig. 4 shows the RMSE performance of our STS-PredNets and baselines versus the prediction range. It can be observed that our STS-PredNets consistently achieve better performance than the baselines. With the increase of the prediction range, the performances of the temporal models (HA, ARIMA and LSTM) drop dramatically, while relatively stable performances are obtained by our STS-PredNets. Moreover, it is noticed that the gap between STS-PredNet and STS-PredNet-C becomes wider for a larger prediction range. This is because the closeness component can capture less useful information for long-term spectrum prediction. By contrast, the daily period and weekly trend patterns in spectrum data are more significant for long-term spectrum prediction and should be paid more attention to.

V. CONCLUSION

In this letter, we propose a novel end-to-end deep-learning-based prediction model entitled STS-PredNet for spatial-temporal-spectral predictive learning of the spectrum data. STS-PredNet employs PredRNN to extract features from spatial, temporal and spectral dimensions. Considering the cyclical patterns observed in the spectrum data, STS-PredNet employs three components with PredRNN to respectively model temporal closeness, daily period and weekly trend, and dynamically aggregates the outputs of the three components according to the contributions of different patterns. We evaluate our STS-PredNet on a real-world spectrum measurement dataset. The experimental results show that our model achieves the state-of-the-art performance and is promising to be applied to spectrum prediction with different prediction ranges.

REFERENCES

[1] X. Xing, T. Jing, Y. Huo, H. Li, and X. Cheng, "Channel quality prediction based on Bayesian inference in cognitive radio networks," in *Proc. IEEE INFOCOM*, Turin, Italy, Apr. 2013, pp. 1465–1473.
[2] G. Ding *et al.*, "Spectrum inference in cognitive radio networks: Algorithms and applications," *IEEE Commun. Surveys Tuts.*, vol. 20, no. 1, pp. 150–182, 1st Quart., 2018.
[3] L. Yu, J. Chen, G. Ding, Y. Tu, J. Yang, and J. Sun, "Spectrum prediction based on taguchi method in deep learning with long short-term memory," *IEEE Access*, vol. 6, pp. 45923–45933, 2018.
[4] R. Mennes, M. Claeys, F. A. P. De Figueiredo, I. Jabandžić, I. Moerman, and S. Latré, "Deep learning-based spectrum prediction collision avoidance for hybrid wireless environments," *IEEE Access*, vol. 7, pp. 45818–45830, 2019.
[5] B. S. Shawel, D. H. Woldegebreal, and S. Pollin, "Convolutional LSTM-based long-term spectrum prediction for dynamic spectrum access," in *Proc. 27th Eur. Signal Process. Conf. (EUSIPCO)*, A Coruña, Spain, Sep. 2019, pp. 1–5.
[6] F. Lin, J. Chen, J. Sun, G. Ding, and L. Yu, "Cross-band spectrum prediction based on deep transfer learning," *China Commun.*, vol. 17, no. 2, pp. 66–80, Feb. 2020.
[7] L. Yu *et al.*, "Spectrum availability prediction for cognitive radio communications: A DCG approach," *IEEE Trans. Cognit. Commun. Netw.*, vol. 6, no. 2, pp. 476–485, Jun. 2020.
[8] S. Rajendran *et al.*, "Electrosense: Open and big spectrum data," *IEEE Commun. Mag.*, vol. 56, no. 1, pp. 210–217, Jan. 2018.
[9] Y. Wang, M. Long, J. Wang, Z. Gao, and P. S. Yu, "PredRNN: Recurrent neural networks for predictive learning using spatiotemporal LSTMs," in *Proc. Adv. Neural Inf. Process. Syst.*, 2017, pp. 879–888.
[10] J. Sun, L. Shen, G. Ding, R. Li, and Q. Wu, "Predictability analysis of spectrum state evolution: Performance bounds and real-world data analytics," *IEEE Access*, vol. 5, pp. 22760–22774, 2017.
[11] Z. Du, Q. Wu, and P. Yang, "Dynamic user demand driven online network selection," *IEEE Commun. Lett.*, vol. 18, no. 3, pp. 419–422, Mar. 2014.
[12] S. Guo, Y. Lin, S. Li, Z. Chen, and H. Wan, "Deep spatial-temporal 3D convolutional neural networks for traffic data forecasting," *IEEE Trans. Intell. Transp. Syst.*, vol. 20, no. 10, pp. 3913–3926, Oct. 2019.
[13] I. Sutskever, O. Vinyals, and Q. V. Le, "Sequence to sequence learning with neural networks," in *Proc. Adv. Neural Inf. Process. Syst. (NIPS)*, 2014, pp. 3104–3112.
[14] J. Zhang, Y. Zheng, and D. Qi, "Deep spatio-temporal residual networks for citywide crowd flows prediction," in *Proc. 31st AAAI Conf. Artif. Intell.*, San Francisco, CA, USA, Feb. 2017, pp. 1655–1661.
[15] C. Zhang, H. Zhang, D. Yuan, and M. Zhang, "Citywide cellular traffic prediction based on densely connected convolutional neural networks," *IEEE Commun. Lett.*, vol. 22, no. 8, pp. 1656–1659, Aug. 2018.
[16] W. Li, J. Yin, and H. Chen, "Supervised topic modeling using hierarchical Dirichlet process-based inverse regression: Experiments on E-commerce applications," *IEEE Trans. Knowl. Data Eng.*, vol. 30, no. 6, pp. 1192–1205, Jun. 2018.